PHYSICAL REVIEW D VOLUME 42, NUMBER 5 1 SEPTEMBER 1990

Possibility of detection of Higgs boson and precise test of the standard model in e^-e^+ annihilation at $\sqrt{s}=M_Z$: Energy distributions for signal and background

Yoshikazu Yoneda and Osamu Terazawa
Department of Physics, Faculty of Science, Shinshu University, Matsumoto 390, Japan

Minoru Biyajima
Department of Physics, Faculty of Liberal Arts, Shinshu University, Matsumoto 390, Japan
(Received 29 March 1990)

The detectability of the Higgs boson at $\sqrt{s}=M_Z$ is studied, considering the energy distribution of the final leptons. Concise formulas are given for the background process; they will serve as a precise test of the standard model.

I. INTRODUCTION

The Higgs-boson search is one of the most important problems for the standard model.[1] Many authors have studied this problem.[2-12] Previously we have studied it from the point of view of the invariant-mass distribution[10,11] and the collinearity angle-distribution[12] for the signal process

$$e^-+e^+\to Z\to l+\bar{l}+H\ , \tag{1}$$

where e^-, e^+, Z, l, $\bar{l}$, and H are the electron, positron, Z particle, lepton, antilepton, and Higgs boson, respectively. For the background process we have considered

$$e^-+e^+\to\gamma,\quad Z\to f\bar{f}\to l+\bar{l}+X\ , \tag{2}$$

where γ, f, and $\bar{f}$ are the photon, fermion, and antifermion, respectively.

In this paper we investigate the problem of the energy distribution of a lepton pair at $\sqrt{s}=M_Z$ (where $\sqrt{s}$ is the center-of-mass energy and M_Z is the mass of the Z particle), taking into account the advent of SLC (SLAC Linear Collider) and LEP (CERN Large Electron Positron Collider).

In Sec. II, we give the energy distribution for the signal process of (1), and especially we give the concise total cross section although the approximation $\gamma_Z=\Gamma_Z/M_Z=0$ is used, where Γ_Z is the total width of the Z particle. In Sec. III, we give the energy distribution and cross section of the background process (2). In addition to the usual energy distribution, we derive spin-correlated effects which will serve for the precise test of the standard model. Section IV is devoted to numerical calculations and conclusions.

II. CROSS SECTION FOR THE SIGNAL

The Feynman diagram for the signal process of (1) is given in Fig. 1. Other processes such as the vector-boson fusion process are negligible for the energy $\sqrt{s}=M_Z$ with which we will be concerned. The differential cross section at $\sqrt{s}=M_Z$ is given as

$$d\sigma(e^-e^+\to l^-l^+H)=(12\pi/M_Z^2\Gamma_Z^2)\Gamma(Z\to e^-e^+)d\Gamma(Z\to l^-l^+H)\ , \tag{3}$$

where the initial-spin average and the final-spin sum are understood, and

$$d\Gamma(Z\to l^-l^+H)/dx_-dx_+=[g^2(ZZH)/48(2\pi)^3M_Z][a_V^2(Zl)+a_A^2(Zl)]F(x_-,x_+;\gamma_Z)\ , \tag{4}$$

$$F(x_-,x_+;\gamma_Z)=(x_-+x_+-\delta_H^2-1+x_-x_+)/[(2-\delta_H^2-x_--x_+)^2+\gamma_Z^2]\ , \tag{5}$$

$$x_\pm=2E_\pm/M_Z,\quad \delta_H=M_H/M_Z(<1),\quad \gamma_Z=\Gamma_Z/M_Z\ , \tag{6}$$

$$-x_-x_+\le 1-x_--x_+-\delta_H^2\le 0\ , \tag{7}$$

$$g(ZZH)=(g/\cos\theta_W)M_Z,\quad a_V(Zl)=(g/\cos\theta_W)[-T_L(l)/2+Q(l)\sin^2\theta_W],\quad a_A(Zl)=(g/\cos\theta_W)T_L(l)/2\ . \tag{8}$$

Here we have neglected the initial- and final-lepton masses. In the case of $\gamma_Z=0$, Eq. (4) reduces to that of Ref. 8, and we also use the approximation hereafter. The function $F(x_-,x_+;0)$ is symmetric for the variables $x_\pm$ and we are able to integrate this function for the variables x_- or x_+: We have

$$F(x;0)=\int_{\epsilon_H-x}^{(\epsilon_H-x)/(1-x)} dx_+ F(x,x_+;0)=-2-\epsilon_H x+x^2+2/f(x)+(1+x)\ln f(x)\ , \tag{9}$$

where

$$\epsilon_H=1-\delta_H^2\ , \tag{10}$$

$$f(x)=[1-(1+\epsilon_H)x+x^2]/(1-x)\ , \tag{11}$$

and

$$0\le x\le\epsilon_H\ . \tag{12}$$

Furthermore we can integrate Eq. (9):

$$\begin{aligned}F(\gamma_Z=0)&=\int_0^{\epsilon_H}F(x;0)dx\\&=-\tfrac{1}{12}(1-\delta_H^2)(47-13\delta_H^2+2\delta_H^4)+[-1+(6-\delta_H^2)\delta_H^2/4]\ln\delta_H^2\\&\quad+[2\delta_H^2/\sqrt{|D|}+(4-\delta_H^2)\sqrt{|D|}/2]\{\arctan[(2-\delta_H^2)/\sqrt{|D|}]-\arctan(\delta_H^2/\sqrt{|D|})\}\ ,\end{aligned} \tag{13}$$

where

$$|D|=\delta_H^2(4-\delta_H^2)\ . \tag{14}$$

Consequently we have a single-energy distribution from the double-energy distribution of Eq. (4):

$$d\Gamma(Z\to l^-l^+H;\gamma_Z=0)/dx=\Gamma(Z\to l^-l^+H;\gamma_Z=0)n(x)\ , \tag{15}$$

where

$$\Gamma(Z\to l^-l^+H;\gamma_Z=0)=[g^2(ZZH)/48(2\pi)^3M_Z][a_V^2(Zl)+a_A^2(Zl)]F(\gamma_Z=0) \tag{16}$$

and

$$n(x)=F(x;\gamma_Z=0)/F(\gamma_Z=0),\quad \int_0^{1-\delta_H^2}dx\ n(x)=1\ . \tag{17}$$

The function $n(x)$ is the normalized energy distribution.

Although Eqs. (13) and (15) are obtained for $\gamma_Z=0$, they are very concise expressions, compared with an expression of Ref. 6.

III. CROSS SECTION FOR THE BACKGROUND

The Feynman diagram for the background process of (2) is given in Fig. 2. At $\sqrt{s}=M_Z$, the interference term is zero, and the photon- ($\gamma-$) exchange process is suppressed by the factor $(\Gamma_Z/M_Z)^2$ against the Z-exchange process, so we do not consider it hereafter. The other background such as the two-photon process will be rejected considering the invariant-mass distribution, so we do not consider it either.

Following the procedure which was given in Ref. 12, we are able to obtain the differential cross section after some calculations by using the narrow-width approximation (NWA) for the intermediate f and $\bar{f}$ particles:

$$\begin{aligned}&[1/B(a)^2\sigma_{ZZ}(s)]d\sigma_{ZZ}(e^-e^+\to l\bar{l}X;\delta=0)^{(a)}_{\rm NWA}/dx\,dx'\\&\quad=n_1^{(a)}(x)n_1^{(a)}(x')+(1/I(\alpha=0))\{\alpha(a)^2[a_V^2(Zf)(1+\beta^2)/\beta^2+2a_A^2(Zf)]n_2^{(a)}(x)n_2^{(a)}(x')\\&\qquad-4\alpha(a)a_V(Zf)a_A(Zf)[n_2^{(a)}(x)n_1^{(a)}(x')+n_1^{(a)}(x)n_2^{(a)}(x')]\}\ ,\end{aligned} \tag{18}$$

where a = down or up particles.

On the left-hand side of Eq. (18),

$$\sigma_{ZZ}(s)=(24\pi|D(s,Z)|^2)^{-1}[a_V^2(Ze)+a_A^2(Ze)]s\beta I(\alpha=0) \tag{19}$$

is the total cross section for the process $e^-+e^+\to Z\to f+\bar{f}$,

$$I(\alpha=0)=(3-\beta^2)a_V^2(Zf)+2\beta^2a_A^2(Zf)\ , \tag{20}$$

$$D(s,Z)=s-M_Z^2+i\Gamma_Z M_Z \ , \tag{21}$$

$$\sqrt{s}=M_Z, \quad \beta=[1-4(M_f/M_Z)^2]^{1/2} \ , \tag{22}$$

and $B(a)$ is the branching ratio of the f particle,

$$x=2E_1\sqrt{x_0}/M_f, \quad x'=2E_1'\sqrt{x_0}/M_f, \quad x_0=(1-\beta)/(1+\beta) \ . \tag{23}$$

In the derivation of Eq. (18), we have made use of the approximation

$$\delta=(M_f'/M_f)^2=0 \ . \tag{24}$$

Then the asymmetry parameter α is

$$\alpha=-\tfrac{1}{3} \text{ for down particles}, \quad \alpha=1 \text{ for up particles} \ . \tag{25}$$

On the right-hand side of Eq. (18), $n_1^{(a)}$ and $n_2^{(a)}$ are the normalized energy distribution and are given as follows.

For the down particles, we have

$$n_1^{(d)}(x)=[2(1+\beta)/3(1-\beta)^3][9(1-\beta)x^2-2(3+\beta^2)x^3]\theta(x_0-x)\theta(x) + [(1+\beta)/6\beta](1-x)(5+5x-4x^2)\theta(1-x)\theta(x-x_0) \ , \tag{26a}$$

$$\int_0^1 dx\, n_1^{(d)}(x)=1 \ ; \tag{26b}$$

$$n_2^{(d)}(x)=[2(1+\beta)\beta^2/3(1-\beta)^3][9(1-\beta)x^2-8x^3]\theta(x_0-x)\theta(x) + [(1+\beta)/6\beta][5-12(1+\beta)x+9(1+2\beta)x^2-2(1+3\beta)x^3]\theta(1-x)\theta(x-x_0) \ , \tag{27a}$$

$$\int_0^1 dx\, n_2^{(d)}(x)=0 \ . \tag{27b}$$

For the up particles, we have

$$n_1^{(u)}(x)=[4(1+\beta)/(1-\beta)^3][3(1-\beta)x^2-(3+\beta^2)x^3]\theta(x_0-x)\theta(x)+[(1+\beta)/\beta](1-x)^2(1+2x)\theta(1-x)\theta(x-x_0) \ , \tag{28a}$$

$$\int_0^1 dx\, n_1^{(u)}(x)=1 \ ; \tag{28b}$$

$$n_2^{(u)}(x)=[4(1+\beta)\beta^2/(1-\beta)^3][3(1-\beta)x^2-4x^3]\theta(x_0-x)\theta(x)+[(1+\beta)/\beta](1-x)^2[1-(1+3\beta)x]\theta(1-x)\theta(x-x_0) \ , \tag{29a}$$

$$\int_0^1 dx\, n_2^{(u)}(x)=0 \ . \tag{29b}$$

The functions $n_1^{(d)}(x)$ and $n_1^{(u)}(x)$ are just the ones which were given in Refs. 13 and 14.

By integrating Eq. (18) with respect to x or x', we obtain the single-energy distribution

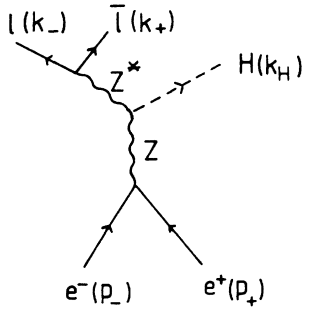

FIG. 1. Feynman diagram of process (1).

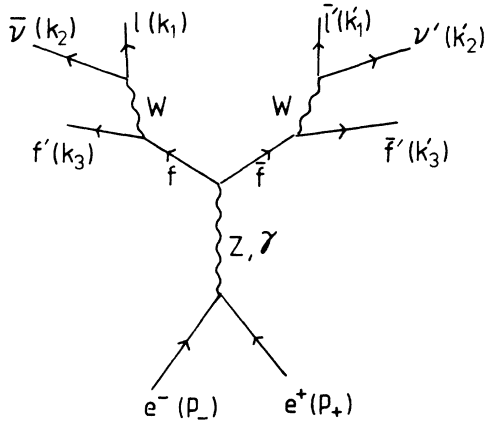

FIG. 2. Feynman diagram of process (2).

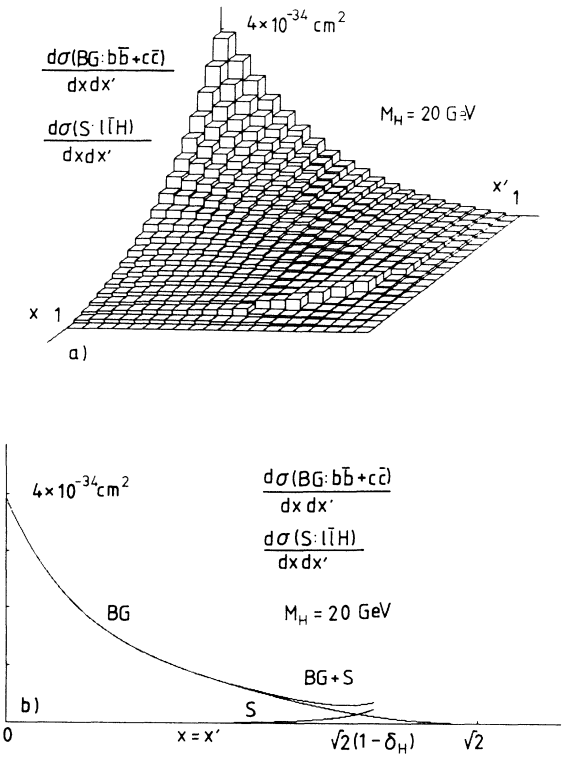

FIG. 3. (a) Double-energy distributions of the background and the signal with $M_H = 20$ GeV. (b) Those types of behavior on the diagonal line, $x = x'$.

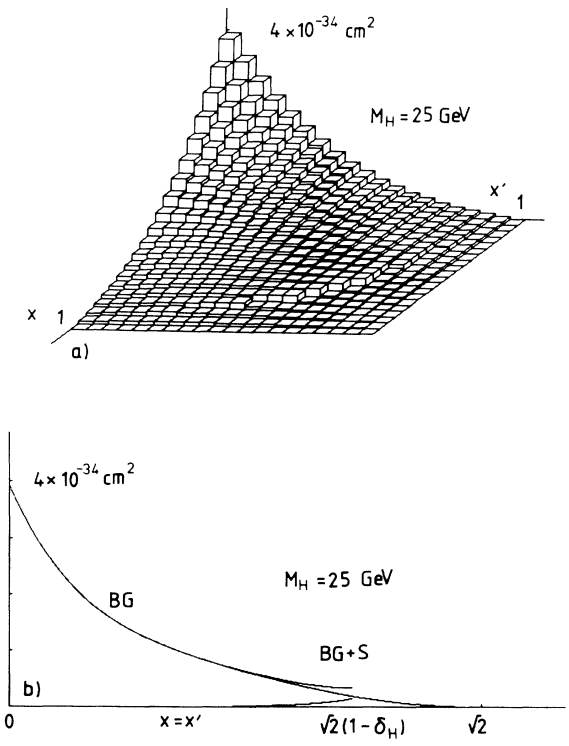

FIG. 4. Same as Fig. 3 for $M_H = 25$ GeV.

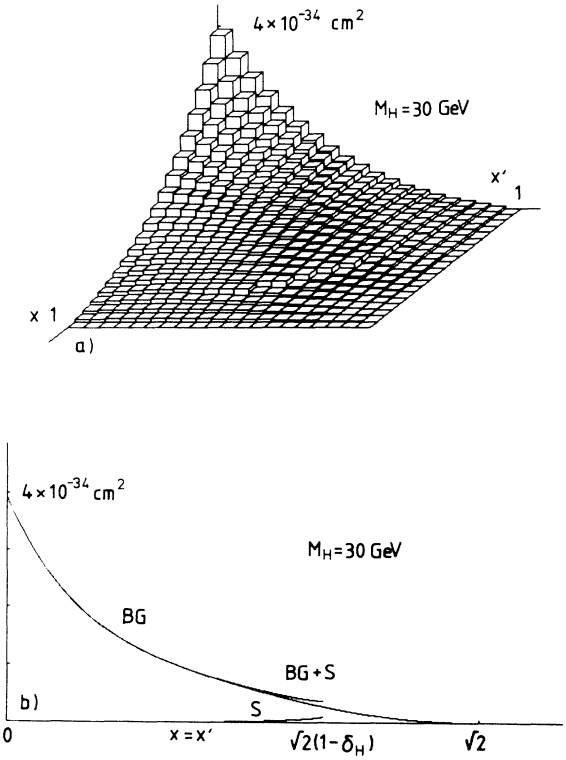

FIG. 5. Same as Fig. 3 for $M_H = 30$ GeV.

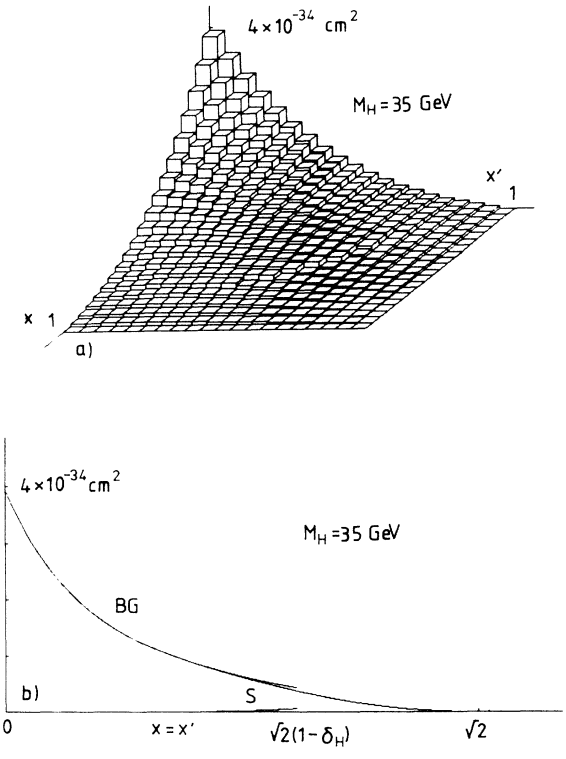

FIG. 6. Same as Fig. 3 for $M_H = 35$ GeV.

$$[1/B(a)^2\sigma_{ZZ}(s)]d\sigma_{ZZ}(e^-e^+\to l\bar{l}X;\delta=0)^{(a)}_{\mathrm{NWA}}/dx$$
$$=n_1^{(a)}(x)-4\alpha(a)a_V(Zf)a_A(Zf)/I(\alpha=0)n_2^{(a)}(x)\ . \tag{30}$$

The second term of Eqs. (18) and (30) is the effect of the spin correlation[15] and will serve as a precise test of the standard model. (More precisely we must evaluate the effect of $\delta\neq 0$. This will be given elsewhere. In the case of the collinearity-angle distribution it was given in Ref. 12.)

Numerical estimations will be given in the next section.

IV. NUMERICAL CALCULATIONS AND CONCLUSIONS

A. Numerical calculations

The Higgs boson decays predominantly to heavy-fermion pairs, so the final-state configuration of the signal will be

$$e^-+e^+\to l+\bar{l}+H\to l+\bar{l}+b\bar{b}\ , \tag{31}$$

where b and $\bar{b}$ are b quark and antiquark, respectively. As for the background of τ lepton,

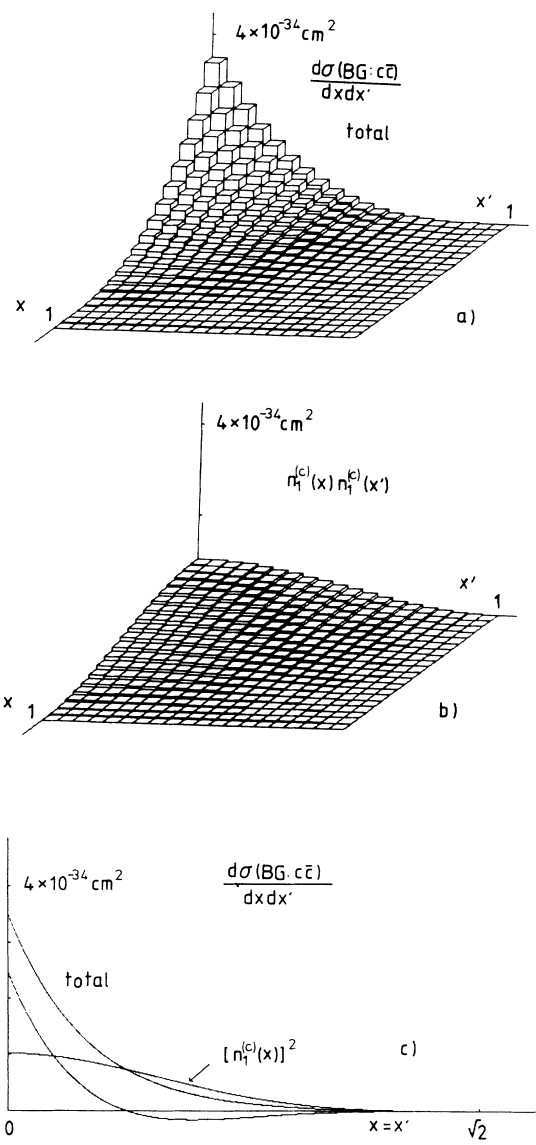

FIG. 7. The double-energy distribution of background of $c\bar{c}$. (a) Total of the right-hand side (RHS) of Eq. (18). (b) The first term of the RHS of Eq. (18). (c) Types of behavior of the diagonal line. $x=x'$.

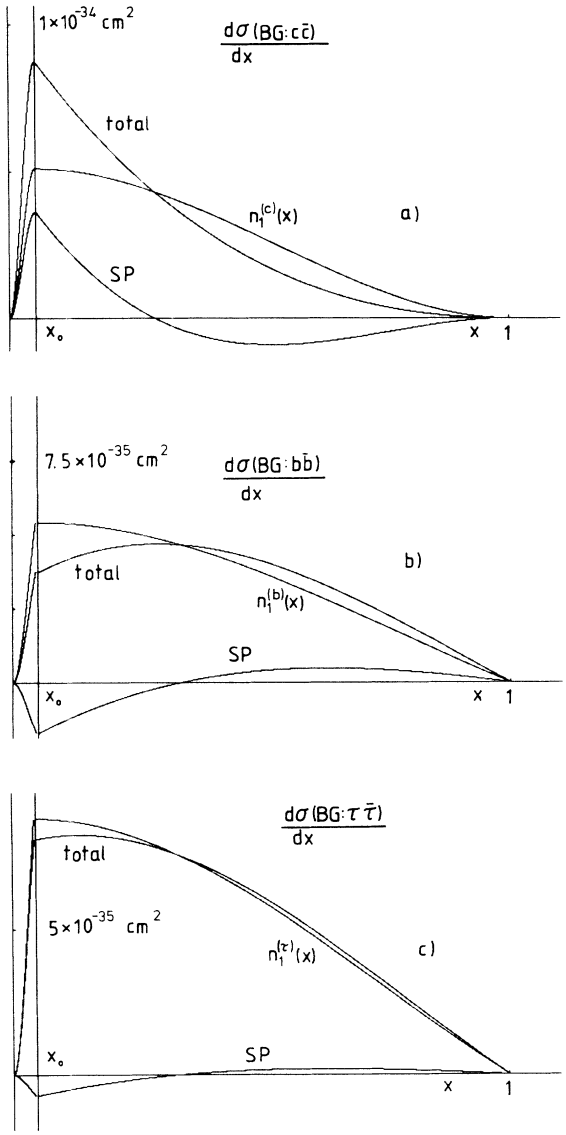

FIG. 8. The single-energy distribution of the background. $x_0=(1-\beta)/(1+\beta)$. It should be noticed that different scales are used for $x<x_0$ and $x_0<x$, because x_0 is very small. SP denotes the spin-correlation effect. (a) $f=c$, (b) $f=b$, and (c) $f=\tau$.

$$e^- + e^+ \to \tau\bar{\tau} \to l + \bar{l} + \text{missing energy} ,$$
$$\to l(\bar{l}) + \text{hadrons} + \text{missing energy} ,$$
$$\to \text{hadrons} + \text{missing energy} . \quad (32)$$

Then we can discriminate this background from the signal. The backgrounds of charm quark c and b remain for the detection of the Higgs boson. In our calculations, we use the values

$$B(c)=0.11, \quad B(\tau)=0.17, \quad \text{and } B(b)=0.11 . \quad (33)$$

In Figs. 3–5, we depict the double-energy distributions of the signal, Eq. (3) for $M_H=20$, 25, and 30 GeV (see Refs. 16 and 17), and the background, Eq. (18) with $f=c$ and b, respectively. Values at the origin are apparent due to $x_0 \cong 0$. (See Fig. 8.) As $x_\pm \sim x, x'$, we use variables x and x' in Figs. 3–7.

As you see in these figures, there are sharp steps at the edge of the Dalitz contour. From these types of behavior we may expect the detection of the Higgs boson with the mass range 20 GeV $\leq M_H \leq$ 30 GeV, at $\sqrt{s}=M_Z$.

As you see in Fig. 6, for 35 GeV $\leq M_H \leq$ 45 GeV, the step, i.e., the signal, disappears.

In Fig. 7 we show the double-energy distribution of the background of $c\bar{c}$. These figures are available for the test of the standard model.

In Fig. 8 we depict the single-energy distributions of the background. As you see in the figures, the spin-correlation effect is fairly large. This will also serve as the precise test of the standard model.

B. Conclusions

(1) The single-energy distribution of the signal, Eq. (15), is derived.

(2) The double- and single-energy distributions of the background, Eqs. (18) and (30), are derived. As you see in Figs. 7 and 8, the spin-correlation effect is fairly large and it will serve as the precise test of the standard model.

(3) The Higgs boson with the mass range 20 GeV $\leq M_H \leq$ 30 GeV can be detected from the double-energy distributions at SLC and LEP, if it is in this mass range.

ACKNOWLEDGMENTS

This work was supported in part by the Japanese Grant in Aid for Science Research Fund of the Ministry of Education, Science and Culture (No. 01540240). We would like to thank E.W.N. Glover (CERN and Fermilab) and K. Hikasa (KEK) for useful conversations.

[1] S. Weinberg, Phys. Rev. Lett. **19**, 1264 (1967); A. Salam, in *Elementary Particle Theory: Relativistic Group and Analyticity (Nobel Symposium No. 8)*, edited by N. Svartholm (Almqvist and Wiksell, Stockholm, 1968), p. 367.

[2] E. Ma and J. Okada, Phys. Rev. D **20**, 1052 (1979).

[3] D. R. T. Jones and S. T. Petcov, Phys. Lett. **84B**, 440 (1979).

[4] R. J. Kelly and T. Shimada, Phys. Rev. D **23**, 1940 (1981).

[5] R. Kleiss, Phys. Lett. **141B**, 261 (1984).

[6] F. A. Berend and R. Kleiss, Nucl. Phys. **B260**, 32 (1985).

[7] D. A. Dicus and S. D. Willenbrock, Phys. Rev. D **32**, 1642 (1985).

[8] P. Kalyniak, J. N. Ng, and P. Zakarauskas, Phys. Rev. D **29**, 502 (1984).

[9] R. Bates and J. N. Ng, Phys. Rev. D **32**, 51 (1985).

[10] T. Morioka, M. Biyajima, and O. Terazawa, Prog. Theor. Phys. **76**, 1089 (1986).

[11] M. Biyajima, K. Shirane, and O. Terazawa, Phys. Rev. D **36**, 2161 (1987).

[12] O. Terazawa and M. Biyajima, Phys. Rev. D **39**, 736 (1989); **40**, 922(E) (1989). In Eq. (6) the numerator of the integrand should contain x^2. Moreover, we used $M_\tau=1.78$ GeV in Eq. (27).

[13] K. Fujikawa and N. Kawamoto, Phys. Rev. D **14**, 59 (1976).

[14] A. Pais and S. B. Treiman, Phys. Rev. D **14**, 295 (1976).

[15] Y. S. Tsai, Phys. Rev. D **4**, 2821 (1971).

[16] OPAL Collaboration, Phys. Lett. B **236**, 224 (1990).

[17] ALEPH Collaboration, D. Decamp *et al.*, Phys. Lett. B **236**, 233 (1990).